Theoretical Study of Pu and Cs Incorporation in a Mono-silicate Neodymium Fluoroapatite $Ca_9Nd(SiO_4)(PO_4)_5F_2$

C. Meis,*,† J. D. Gale,‡ L. Boyer,§ J. Carpena,|| and D. Gosset⊥

Commissariat à l'Energie Atomique, Centre d'Etudes de Saclay, DCC/DPE/SPCP, Bât 125, 91191 Gif-sur-Yvette, France, Department of Chemistry, Imperial College of Science, Technology and Medicine, South Kensington SW7 2AY, U.K., Faculté des Sciences de Limoges, SPCTS. 123, Avenue Albert Thomas, 87060 Limoges Cedex, France, Commissariat à l'Energie Atomique, Centre d'Etudes de Cadarache, DCC/DESD/SEP, Bât 307, 13108 St Paul-lez-Durance Cedex, France, and Commissariat à l'Energie Atomique, Centre d'Etudes de Saclay, DRN/DMT/SEMI/LEMA, Bât 524. 91191 Gif-sur-Yvette, France

Received: January 6, 2000; In Final Form: March 10, 2000

In the context of nuclear waste disposal, the possibility of incorporating selectively plutonium and cesium in a mono-silicate neodymium-fluoroapatite $Ca_9Nd(SiO_4)(PO_4)_5F_2$ (britholite) is investigated. For this purpose, a force field for the modeling of fluoroapatite $Ca_{10}(PO_4)_6F_2$ is established based upon the experimental data of crystallographic parameters and elastic constants. To test further the validity of the potentials, the constant pressure specific heat for $Ca_{10}(PO_4)_6F_2$ is measured and compared to the calculated values. Neodymium ions and silicate groups are introduced in the fluoroapatite structure using transferable potentials to obtain the neodymium-britholites $Ca_{10-y}Nd_y(SiO_4)_y(PO_4)_{6-y}F_2$. The force field accuracy is tested by comparing the calculated and experimental values for the lattice parameters and volumes with respect to y ($1 \leq y \leq 6$). Plutonium and cesium are introduced separately in $Ca_9Nd(SiO_4)(PO_4)_5F_2$ also using transferable potentials. The bulk modulus B and the specific heats, C_P and C_V, of the resulting structures are calculated. The cases of trivalent and tetravalent plutonium have been studied by considering, respectively, the following compositions: $Ca_9Nd_{1-x}(Pu^{3+})_x(SiO_4)(PO_4)_5F_2$ and $Ca_{9.25}(Pu^{4+})_{0.25}Nd_{0.5}(SiO_4)(PO_4)_5F_2$. In both cases plutonium is found to substitute for calcium Ca(2), which is seven coordinated, by six oxygen ions and a fluorine. Conversely, cesium, which is introduced in the following structure $Ca_{9.5}Cs_{0.5}Nd_{0.5}(SiO_4)(PO_4)_5F_2$, will substitute for Ca(1) as well as for Ca(2), with a slight preference for Ca(1) which is nine oxygen coordinated. The activation energies for the lattice migration of Pu and Cs are also calculated in the presence of calcium vacancies.

Introduction

Britholites are phospho-silicate apatites containing various rare earth elements and having the general composition $Ca_{10-y}(R.E.)_y(SiO_4)_y(PO_4)_{6-y}(F,OH)_2$ ($1 \leq y \leq 6$) where R.E. = La, Ce, Pr, Nd, Pm, Sm, Eu, and Gd. Natural analogues of such apatites contain important amounts of uranium and thorium while some britholites found in the Oklo natural reactor site have retained ^{235}U, issued from the decay of ^{239}Pu incorporated during crystallization, as well as a high variety of fission products in their structure over geological time periods.[1] Actinides substitute for rare earth elements, at calcium sites, while fission products are also readily incorporated. Although the Oklo apatites have been subject to significant α-decay doses for more than two billion years they are mostly found in a highly crystalline state.[2] Hence, the Oklo britholites are generally considered as the most convincing demonstration of the apatite structure stability and durability under radiation conditions in a geologic environment. Furthermore, studies on geological fluoro-phospho-calcic apatites have shown that radiation-induced defects can be annealed at very low temperature (∼65 °C).[3] This inherent capacity of the apatite structure has also been demonstrated recently by ion beam experiments.[4,5] Taking into account these properties, apatites have been proposed for the immobilization of Pu and high-level wastes.[6−8]

Fluoroapatite $Ca_{10}(PO_4)_6F_2$ has been revealed to be among the most radiation-resistant materials for temperatures above 70 °C.[3,9] However, this property considerably diminishes when significant amount of chlorine are substituted for fluorine and also when increasing numbers of silicates are substituted for phosphates while rare earth elements are substituted for calcium to charge compensate.[10] This was initially observed on the magmatic britholites found in In Ouzzal, (Hoggar shield, Algeria), containing up to 50% p.w. of rare earth elements (La, Ce, Nd), of U and Th.[11] Ion beam radiation experiments have confirmed this observation showing the decrease of the irradiation dose for amorphization, at low temperature, with the increase of the silicate and rare earth elements concentration.[4,5,9] Furthermore, recent luminescence studies[12] have revealed the high resistance of fluoride phospho-apatite structure mainly due to the strong bonds between lanthanides and fluorine anions as well as to the rigidity of the PO_4 groups.

Consequently, a potential candidate for actinides immobilization should preferably be a low silicate fluoro-britholite

* Author to whom correspondence should be addressed.
† Commissareat à l'Energie Atomique, Centre d'Etudes de Saclay, DCC/DPE, SPCP.
‡ Imperial College of Science, Technology and Medicine.
§ Faculté des Sciences de Limoges.
|| Commissariat à l'Energie Atomique, Centre d'Etudes de Cadarache.
⊥ Commissariat à l'Energie Atomique, Centre d'Etudes de Saclay, DRN/DMT/SEMI/LEMA.

10.1021/jp000096j CCC: $19.00
Published on Web 05/12/2000

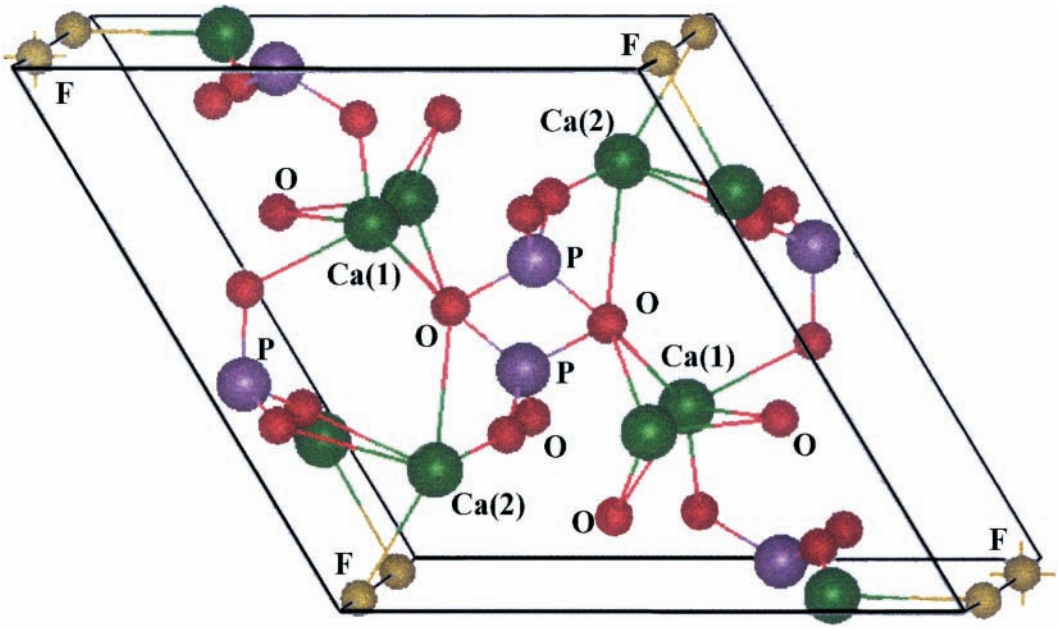

Figure 1. Fluoroapatite $Ca_{10}(PO_4)_6F_2$ unit cell. Ca(1) and Ca(2) denote calcium at sites 1 and 2, respectively.

$Ca_{10-y}(R.E.)_y(SiO_4)_y(PO_4)_{6-y}F_2$ ($y \leq 1$).[8] In this paper we present experimental results on the synthesis and characterization of neodymium-britholites $Ca_{10-y}Nd_y(SiO_4)_y(PO_4)_{6-y}F_2$, and also carry out a computational study using interatomic potential modeling in order to investigate the possibility of introducing Pu and Cs selectively in a mono-silicate Nd-britholite $Ca_9Nd(SiO_4)(PO_4)_5F_2$. The neodymium choice is simply based on the fact that the ionic radius of Nd^{3+} and Pu^{3+} are almost identical. The bulk modulus B and the specific heats, C_P and C_V, of the Pu- and Cs-doped Nd-britholites are calculated and the lattice migration energies for these radionuclides have been estimated.

I. Fluoroapatite $Ca_{10}(PO_4)_6F_2$ Force Field

Fluoroapatite occurs naturally as a mineral and can be synthesized easily. [13] The space group is $P6_3/m$ and the unit cell is hexagonal. As represented in Figure 1, calcium ions are situated in two different sites, Ca(1) at site 1 which is coordinated to nine oxygens and Ca(2) at site 2 which is 7-fold coordinated by six oxygen ions and a fluorine. The Ca(2) ions are distributed in a hexagonal spiral configuration along the *c* axes forming tunnels of an approximate diameter of 4 Å whose center is occupied by an array of fluorine anions, a typical characteristic of the apatite structure. Previous studies have revealed that the structural differences between the natural and synthetic fluoroapatites are not significant.[13] However, more recent experiments[14] have shown that differences up to 1% on the lattice parameters can be obtained depending on the method of synthesis and the purity of the initial compounds used. For our study we shall use the data for synthetic apatites published in references.[14,15]

The fluoroapatite structure can be modeled by considering two-body ionic short-range interaction potentials of the well-known Buckingham type, supplementing the Coulomb interactions. This form is composed of a Born−Mayer repulsive exponential term and an r^{-6} attractive one, $E_{ij} = A_{ij}\exp(-r_{ij}/\rho_{ij}) - C_{ij}/r_{ij}^6$, where r_{ij} is the distance between ion *i* and *j*. For the sake of simplicity, cation−cation interactions, other than electrostatic ones, are set to zero and only anion−cation and anion−anion potentials are established. Furthermore, a harmonic three-body short-range interaction potential of the type $E_{ijk} = 1/2k_{ijk}(\theta - \theta_0)^2$ is introduced in order to better represent the tetrahedral configuration of oxygen ions around phosphorus. The oxygen ion polarizability is taken into account by using the classical model of Dick and Overhauser,[16] according to which a harmonic constant K_P characterizes the interaction between the core, corresponding roughly to the nucleus charge shielded by the inner electrons, and the shell, representing the charge of the outer electrons of the ion: $E_P = 1/2K_P r_{core-shell}^2$. The potential parameters $\{A_{ij}, \rho_{ij}, C_{ij}, K_P, k_{ijk}, \theta_0\}$ corresponding to all the above interactions involved in the fluoroapatite structure have been fitted to the experimental data of lattice parameters and ionic positions,[14,15] as well as to the elastic matrix elements and the bulk modulus.[17] The fitting is based on a least squares procedure minimizing the sum of the squares of the differences between the experimental values and the calculated ones.[18] The Born−Mayer terms of the oxygen−oxygen, fluorine−fluorine, and oxygen−fluorine, two-body interactions are fixed at the values published previously.[19−21] However, the corresponding attractive parameters *C* are fitted. All calculations were performed using the program GULP.[22] The final potentials obtained by the fitting are represented in Table 1, while the physical properties involved in this procedure and obtained by the established force field are represented in Table 2.

TABLE 1: Potentials Parameters and Ionic Charges for Fluoroapatite $Ca_{10}(PO_4)_6F_2$[a,b]

interaction	*A* (eV)	ρ (Å)	*C* (eV Å^6)	K_P (eV Å^{-2})	cutoff (Å)
$O_{shell}-O_{shell}$	22764	0.1490	32.58		12
$O_{shell}-P_{core}$	836	0.3513	0		10
$O_{shell}-Ca_{core}$	1288	0.3316	0		10
$O_{shell}-F_{core}$	198	0.1110	0		10
$F_{core}-P_{core}$	697	0.2389	0		10
$F_{core}-Ca_{core}$	2031	0.2711	0		10
$F_{core}-F_{core}$	1128	0.2753	0		10
$O_{core}-O_{shell}$				98.67	0.7

[a] Three-body harmonic: $k_{Oshell-Pcore-Oshell} = 2.840$ eV rad^{-2}; $\theta_0 = 109.5$ deg. [b] Charges: O_{core}: +0.860; O_{shell}: −2.860; F_{core}: −1; P_{core}: +5; Ca_{core}: +2.

The calcium−oxygen distances as well as the phosphate group bond angles of the relaxed fluoroapatite structure are given in Table 3 and compared to the experimental values,[14] showing reasonable agreement on the whole.

TABLE 2: Fluoroapatite Properties[14,15,17] Used for the Derivation of Potential Parameters. The Final Calculated Values Obtained Using the Force Field Given in Table 1 Are also Given

$Ca_{10}(PO_4)_6F_2$	experiment	calculated	%
a (Å)	9.374(3)	9.3688	−0.05
c (Å)	6.888(1)	6.8694	−0.27
V (Å^3)	524.2(5)	522.2	−0.38
c_{11}(10^{11} dyn/cm^2)	16.67	16.46	−1.2
c_{13}	6.55	6.03	−7.9
c_{33}	13.96	14.55	4.2
c_{55}	6.63	5.47	−17.5
bulk modulus B(GPa)	98	91.8	−6.3

To check further the quality of the force field, we have measured the constant pressure specific heat C_P in the temperature range from 20 to 800 °C, and compared these values to the calculated one. The C_P measurements have been performed on a SETARAM DSC 111 differential calorimeter calibrated with a sapphire NBS standard. A temperature step program has been chosen. The values we obtain are then the mean specific heat values on a given step:

$$C_P[T_1 + \Delta T/2] = \frac{1}{T_2 - T_1}\int_{T_1}^{T_2} Cp(T)\,dT \qquad (1)$$

with a constant step $\Delta T = T_2 - T_1 = 20$ °C on the whole temperature range. This allows a better accuracy for the specific heat values but makes impossible the precise location of material enthalpy changes (desorption, phase transformations, etc.). The measurements were performed in an inert gas flow (argon) with the fluoroapatite powders (of about 100 mg) in alumina crucibles. The fluoroapatite samples have been obtained by the sintering route at 1100 °C at atmospheric pressure. Water was sorbed during cooling of the structures and this is clearly shown in Figure 2, where a first measurement leads to quite abnormal C_P(T) curves (peaks, plateau). A second measurement was then performed, without removing the samples from the inert atmosphere of the furnace to prevent re-hydration. The obtained curves show a normal behavior on the whole. After replacing the samples 15 min in air, new peaks appear at low temperature, corresponding to hydration but the high-temperature part of the curves shows no significant changes. The mean value of the second and third measurements is reported in Figure 2.

Theoretically, the constant pressure specific heat can be calculated by the well-known expression

$$C_P = T\left.\frac{\partial S_{vib}}{\partial T}\right|_P \qquad (2)$$

where the vibration entropy S_{vib} at a given temperature T is obtained by the partition function Z_{vib} according to the relation:

$$S_{vib} = k_B \ln Z_{vib} + k_B T\frac{\partial}{\partial T}(\ln Z_{vib}) \qquad (3)$$

The partition function is given by

$$Z_{vib} = \sum_{k\ \text{points}=10} g_k \sum_{i=1}^{3N} \exp(-h\nu_i/k_B T) \qquad (4)$$

where ν_i are the phonon frequencies summed over a grid covering 10 symmetry-unique points across the Brillouin zone, excluding the three translational degrees of freedom at the gamma point, g_k being the weight of each grid point. N is the total number of ions in the simulation volume, which is a single unit cell of fluoroapatite $Ca_{10}(PO_4)_6F_2$ with periodic boundary conditions. Also, k_B and k are Boltzmann's and Planck's constants, respectively. The phonon frequencies ν_i are calculated from the eigen-values of the dynamic matrix of the system, corresponding to the Cartesian second derivatives of the energy weighted by the inverse square root of the ion masses.

TABLE 3: Comparison of the Calcium−Oxygen Interatomic Distances and Phosphate Group Bond Angles of the Fluoroapatite Structure to the Experimental Values[14]

dist (Å)−angles (deg)	experiment	calculated
Ca(1)−O(1)	2.400	2.383
Ca(1)−O(2)	2.456	2.437
Ca(1)−O(3)	2.808	2.912
Ca(2)−O(1)	2.672	2.713
Ca(2)−O(2)	2.404	2.418
Ca(2)−O(3)	2.506	2.562
O(1)−P−O(2)	111.52	109.88
O(3)−P−O(2)	107.73	106.85

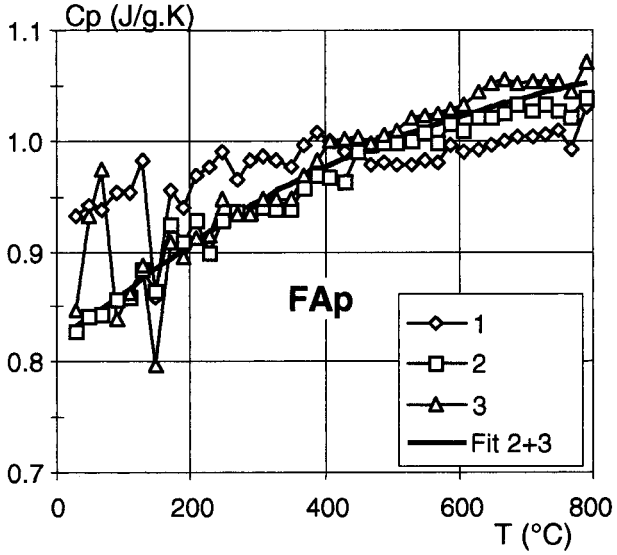

Figure 2. Measurements of the specific heat C_P versus temperature of fluoroapatite $Ca_{10}(PO_4)_6F_2$ (Fap). (1) and (2): successive measurements of the same sample maintained in an inert gas. (3): after 15 min in air. (Fit 2 + 3): polynomial adjustment of 2 + 3 curves.

The polynomial fitting of the calculated and experimental values is plotted in Figure 3. The efficiency of the force field is quite satisfactory as the calculated C_P values are about 4% to 5% lower than the experimental ones for which the estimated uncertainties are of the order of ±3%. The specific heat at constant volume C_V can also be calculated with respect to the temperature, also using the phonon spectra according to the analytical expression:

$$C_V = \sum_{k\ \text{points}=10} g_k \sum_{i=1}^{3N} k_B \left(\frac{h\nu_i}{k_B T}\right)^2 \frac{\exp\left(\frac{h\nu_i}{k_B T}\right)}{\left(\exp\left(\frac{h\nu_i}{k_B T}\right) - 1\right)^2} \qquad (5)$$

The polynomial fitting of the C_V values, also reported in Figure 3, is lower than the calculated one for the C_P, in agreement with thermodynamic principles.

II. Synthesis, Crystal Chemistry, and Force Field for Neodymium-Britholites

We have developed an elaboration process for the synthesis of britholitic ceramics.[8,14] The total substitution of SiO_4 for PO_4

TABLE 4: Calculation of the Lattice Parameters and Volume Variation Following the Solid Solution of Nd in $Ca_{10-y}Nd_y(SiO_4)_y(PO_4)_{6-y}F_2$ ($1 \le y \le 6$)

$Ca_{10-y}Nd_y(SiO_4)_y(PO_4)_{6-y}F_2$	a (Å)	%	c (Å)	%	V (Å^3)	%
$Ca_9Nd(SiO_4)(PO_4)_5F_2$	9.438(9.405)	+0.26	6.851(6.906)	−0.79	526.8(529.0)	−0.41
$Ca_8Nd_2(SiO_4)_2(PO_4)_4F_2$	9.480(9.438)	+0.44	6.888(6.938)	−0.72	533.2(535.2)	−0.35
$Ca_7Nd_3(SiO_4)_3(PO_4)_3F_2$	9.502(9.476)	+0.27	6.926(6.964)	−0.56	538.8(540.1)	−0.22
$Ca_6Nd_4(SiO_4)_4(PO_4)_2F_2$	9.573(9.494)	+0.83	6.901(6.981)	−1.14	542.1(544.9)	−0.49
$Ca_5Nd_5(SiO_4)_5(PO_4)F_2$	9.592(9.508)	+0.88	6.913(6.996)	−1.18	545.3(547.7)	−0.44
$Ca_4Nd_6(SiO_4)_6F_2$	9.591(9.527)	+0.68	6.939(7.013)	−1.06	548.9(551.2)	−0.42

[a] Comparisons to the experimental values are given in parentheses.[14]

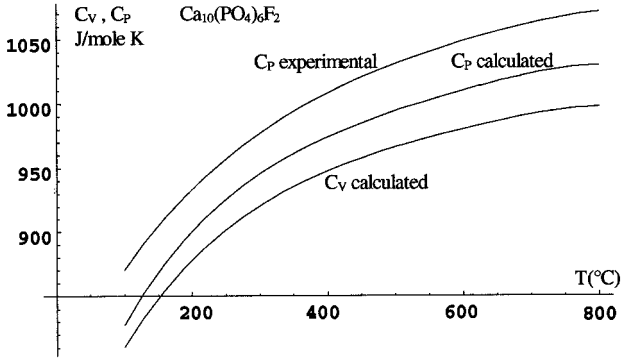

Figure 3. Experimental and calculated values of the fluoroapatite specific heat at constant pressure, C_P, versus temperature. The experimental uncertainties are ±3%. The calculated C_V is also reported.

in the apatite lattice appears to be possible. Detailed X-ray diffraction studies on $Ca_{10-y}Ln_y(SiO_4)_y(PO_4)_{6-y}F_2$, with $1 \le y \le 6$, and Ln (a lanthanide ion), confirms that a continuous solid solution exists between the two limiting compounds $Ca_{10}(PO_4)_6F_2$ and $Ca_4Ln_6(SiO_4)_6F_2$.[11] This solid solution follows the Vegard's law.[14,15]

Neodymium britholites were obtained from an initial mixture of CaF_2, $Ca_2P_20_7$, $CaCO_3$, Nd_2O_3, and SiO_2, with stoichiometry according to the equation

$$3CaCO_3 + [(6-y)/2]\,Ca_2P_2O_7 + CaF_2 + (y/2)Nd_2O_3 + ySiO_2 \rightarrow Ca_{10-y}Nd_y(SiO_4)_y(PO_4)_{6-y}F_2 + 8CO_2 \quad (6)$$

Heating to 1700 K with a ramp rate of 300 K/h was performed. After an annealing time of 6 h, the temperature was decreased to ambient temperature at a rate of 50 K/min. X-ray diffraction studies[14] confirmed that the crystals pertained to the apatite structure, with the group symmetry $P6_3/m$, while the different lattice parameters were obtained using α-alumina as an internal reference and presented in parentheses in Table 4.

From a theoretical point of view, the Nd-britholite structures for $1 \le y \le 6$ can be obtained by substituting successively a pair of (Ca^{2+}, $[PO_4]^{3-}$) for a pair of (Nd^{3+}, $[SiO_4]^{4-}$) in the established fluoroapatite model. In the absence of sufficient experimental data to fit potentials directly to the Nd-britholites properties (elastic matrix elements, dielectric constants, etc.), we have optimized the corresponding interactions for Si and Nd in other crystals and then transferred the established potentials into the above model of the fluoroapatite structure. Thus, the silicate interactions consisting of a $Si_{core}-O_{shell}$ two-body Born−Mayer potential and an $O_{shell}-Si_{core}-O_{shell}$ three-body harmonic one have been optimized in zircon ($ZrSiO_4$)[23] while the $Si_{core}-F_{core}$ interaction was determined in silicon fluoride (SiF_4). In the same way, the $Nd_{core}-O_{shell}$ interaction has been optimized in neodymium sesquoxide (Nd_2O_3) and the $Nd_{core}-F_{core}$ one in neodymium fluoride (NdF_3). The potential parameters used for the above interactions are given in Table 5. It is worth noticing that the established $Nd_{core}-O_{shell}$ Born−Mayer potential is very close to the one published previously.[24]

TABLE 5: Born−Mayer Potential Parameters Introduced into the Fluorapatite $Ca_{10}(PO_4)_6F_2$ Model To Get the Nd-Britholite Structure $Ca_{10-y}Nd_y(SiO_4)_y(PO_4)_{6-y}F_2$. The Cutoff for the Two-Body Interactions is 10 Å

interaction	A (eV)	ρ (Å)	structure used for derivation
$O_{shell}-Si_{core}$	1078	0.3237	$ZrSiO_4$ (tetragonal, I41/AMD)
$O_{shell}-Nd_{core}$	1380	0.3604	Nd_2O_3 (trigonal, P-3 M1)
$F_{core}-Si_{core}$	3506	0.2251	SiF_4 (cubic, I-4 3M)
$F_{core}-Nd_{core}$	89596	0.1983	NdF_3 (hexagonal, P-3 C1)

[a] Three-body harmonic, also optimized in zircon: $k_{Oshell-Si-Oshell} = 16.67$ eV rad^{-2}. [b] Charges: O_{core}, +0.860; O_{shell}: −2.860; F_{core}: −1; Nd_{core}: +3; Si_{core}: +4.

In Table 4 are presented the calculated lattice parameters and volumes of the Nd-britholites, applying the potentials of Tables 1 and 5, and they are compared to the experimental values[14] showing good agreement, particularly in the trends. This is mainly due to the fact that the transferred Si and Nd interactions have been established in the various crystal structures under the constraints of transferability conditions. In fact, in all the structures used for that purpose, presented in Table 4, we have considered the same core/shell charges for the oxygen polarizability model, the same $O_{shell}-O_{shell}$ interaction potential, as well as the same $F_{core}-F_{core}$ potential as that used in the fluoroapatite model.

The fact that the $Ca_{10-y}Nd_y(SiO_4)_y(PO_4)_{6-y}F_2$ unit cell volume increases with respect to y is mainly due to the difference between the ionic radius of Ca^{2+} (0.99 Å) and of Nd^{3+} (1.08 Å) as well as to that between the phosphate $[PO_4]^{3-}$ and silicate $[SiO_4]^{4-}$ volumes, the last one being larger as the interatomic distances Si−O [$d_{Si-O} = 1.62$ Å] are longer than those of P−O [$d_{P-O} = 1.53$ Å].

In the case of the mono-silicate Nd-britholite, in which we are mainly interested, it is worth examining whether the established force field can reproduce physical properties other than the structural ones. For that purpose we have studied the preference of Nd^{3+} ions to substitute for calcium at Ca(1) or at Ca(2), by calculating the difference between the free energies at 300 K corresponding to the minimized structures of these two configurations, giving

$$A_{300\ K}[Nd^{3+}\text{ at Ca(1)}] - A_{300\ K}[Nd^{3+}\text{ at Ca(2)}] = +72.5\ \text{kJ/mol} \quad (7)$$

where $A_{300K}[Nd^{3+}$at Ca(1)] is the free energy ($A = U_{lattice} - TS_{vib}$) of the internal energy minimized structure $Ca_9Nd(SiO_4)(PO_4)_5F_2$ when the Nd^{3+} ion substitutes for Ca^{2+} at site Ca(1), and $A_{300\ K}[Nd^{3+}$ at Ca(2)] that when it substitutes for Ca^{2+} at site Ca(2). It appears that neodymium will preferentially occupy the site Ca(2), which is in accordance with all the previous experimental observations.[25−27] Furthermore, Laue diffraction studies on Nd-britholite single crystals, whose chemical analysis by an SX50 CAMECA microprobe revealed it to have the

TABLE 6: Calculated (rounded to the nearest integer) Properties of Fluoroapatite and Nd-Britholites at 300 K

$Ca_{10-y}Nd_y(SiO_4)_y(PO_4)_{6-y}F_2$	B (GPa)	C_V (J/mol K)	C_P (J/mol K)	S_{vib} (J/mol K)
$Ca_{10}(PO_4)_6F_2$	92	726	740	808
$Ca_9Nd(SiO_4)(PO_4)_5F_2$	98	717	733	799
$Ca_8Nd_2(SiO_4)_2(PO_4)_4F_2$	101	713	726	788
$Ca_7Nd_3(SiO_4)_3(PO_4)_3F_2$	104	702	719	778
$Ca_6Nd_4(SiO_4)_4(PO_4)_2F_2$	110	695	713	762
$Ca_5Nd_5(SiO_4)_5(PO_4)F_2$	116	693	708	757
$Ca_4Nd_6(SiO_4)_6F_2$	122	686	701	742

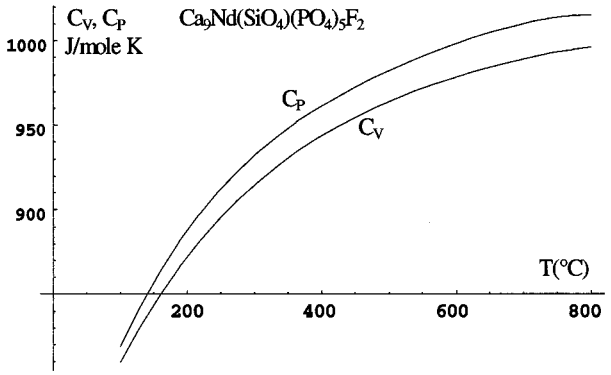

Figure 4. Calculated specific heats, C_P and C_V, for $Ca_9Nd(SiO_4)(PO_4)_5F_2$.

composition $Ca_{9.1}Nd_{0.9}(SiO_4)_{0.9}(PO_4)_{5.1}F_{1.5}0_{0.25}(\square)$, have shown that the neodymium is distributed 17% at site Ca(1) and 83% at Ca(2) while the hexagonal channel which contains the fluorine anions is partially filled by 77% F^- and 13% O^{2-}, the remaining 10% being vacancies ($\square$).[28]

Consequently, the established force field for the Nd-britholites is capable of reproducing the physical properties with useful precision. We have thus calculated, at 300 K, the bulk modulus B, the vibrational entropy S_{vib}, and the specific heats at constant pressure C_P and constant volume C_V, of all the Nd-britholites for $1 \le y \le 6$ (Table 6).

The bulk modulus increases steadily with increasing silicate and neodymium substitutions while the thermodynamic quantities S_{vib}, C_P, and C_V decrease slightly. The specific heat at constant volume and at constant pressure for $Ca_9Nd(SiO_4)(PO_4)_5F_2$, also calculated by using the formalism of eqs 2−5 are represented in Figure 4. They are lower than those of fluoroapatite by 1−2%.

III. Plutonium and Cesium Incorporation in $Ca_9Nd(SiO_4)(PO_4)_5F_2$

According to the synthesis conditions plutonium could be incorporated in the mono-silicate neodymium britholite $Ca_9Nd(SiO_4)(PO_4)_5F_2$ either in the oxidation state +3 or +4. Hence, both cases have to be considered and for that purpose transferable potentials for the interactions $F_{core}-Pu^{3+}{}_{core}$, $F_{core}-Pu^{4+}{}_{core}$, $O_{shell}-Pu^{4+}{}_{core}$, and $O_{shell}-Pu^{3+}{}_{core}$ are established based upon the structural properties of PuF_3, PuF_4, PuO_2, and β-Pu_2O_3, respectively. In the same way, $O_{shell}-Cs_{core}$ and $F_{core}-Cs_{core}$ interactions have been fitted to Cs_2O and CsF, respectively. These potential parameters are given in Table 7.

Chemical immobilization occurs through the process of atomic scale fixation of the radionuclide, as this latter species becomes part of the mineral stoichiometry. Introducing about 6% p.w. of Pu into the mono-silicate Nd-britholite with the trivalent oxidation state, according to the composition $Ca_9(Pu^{3+})_{0.25}Nd_{0.75}(SiO_4)(PO_4)_5F_2$, corresponds to considering

TABLE 7: Potential Parameters Used to Introduce Plutonium and Cesium into the $Ca_{10-y}Nd_y(SiO_4)_y(PO_4)_{6-y}F_2$ Structure. Cutoff = 10 Å

interaction	A(eV)	ρ(Å)	structure used for derivation
$O_{shell}-Cs_{core}$	15085	0.2549	Cs_2O (rhombohedral, R3-MH)
$O_{shell}-Pu^{4+}{}_{core}$	933	0.4042	PuO_2 (cubic, Fm3m)
$O_{shell}-Pu^{3+}{}_{core}$	3250	0.3136	Pu_2O_3 (hexagonal, P-3M1)
$F_{core}-Cs_{core}$	3125	0.2998	CsF (cubic, Fm3m)
$F_{core}-Pu^{4+}{}_{core}$	79439	0.1968	PuF_4 (monoclinic, C2/C)
$F_{core}-Pu^{3+}{}_{core}$	3058	0.2865	PuF_3 (hexagonal, P3−1C)

[a] Charges: O_{core}: +0.860; O_{shell}: −2.860; F_{core}: −1; $Pu^{3+}{}_{core}$: +3; $Pu^{4+}{}_{core}$: +4; Cs_{core}: +1.

TABLE 8: Calculated Lattice Parameters and Volumes for Plutonium-Britholites

$Ca_{10-y}Pu_y(SiO_4)_y(PO_4)_{6-y}F_2$	a (Å)	b (Å)	c (Å)	V (Å^3)
$Ca_9Pu(SiO_4)(PO_4)_5F_2$	9.401	9.376	6.876	525.4
$Ca_8Pu_2(SiO_4)_2(PO_4)_4F_2$	9.422	9.350	6.885	527.7
$Ca_7Pu_3(SiO_4)_3(PO_4)_3F_2$	9.362	9.416	6.896	529.2
$Ca_6Pu_4(SiO_4)_4(PO_4)_2F_2$	9.431	9.424	6.901	532.5
$Ca_5Pu_5(SiO_4)_5(PO_4)F_2$	9.497	9.433	6.906	535.5
$Ca_4Pu_6(SiO_4)_6F_2$	9.419	9.510	6.911	536.1

unit cells of the form $Ca_{72}(Pu^{3+})_2Nd_6(SiO_4)_8(PO_4)_{40}F_{16}$ within periodic boundary conditions. We can investigate the preference of Pu^{3+} ions to substitute for calcium Ca(2) or for Ca(1), by calculating the difference between the free energies corresponding to the minimized configurations

$$A_{300K}[Pu^{3+}\text{at Ca(1)}] - A_{300K}[Pu^{3+}\text{at Ca(2)}] = +93.6\ \text{kJ/mol} \quad (8)$$

where $A_{300K}[Pu^{3+}$ at Ca(1)] is the free energy, at 300 K, of the minimized unit cell $Ca_{72}(Pu^{3+})_2Nd_6(SiO_4)_8(PO_4)_{40}F_{16}$ with the Pu^{3+} substituted for Ca(1), and $A_{300K}[Pu^{3+}$at Ca(2)] that with the Pu^{3+} substituted for Ca(2). As in the case of neodymium, trivalent plutonium has a net preference to substitute for Ca(2), in the fluorine tunnel. This site preference is preserved even when substituting successively Pu^{3+} ions for Nd^{3+} until the mono-silicate Pu-britholite $Ca_9Pu(SiO_4)(PO_4)_5F_2$ is arrived at for which we have

$$A_{300K}[Pu^{3+}\text{at Ca(1)}] - A_{300K}[Pu^{3+}\text{at Ca(2)}] = +13.5\ \text{kJ/mol} \quad (9)$$

where the unit cell here is simply $Ca_9Pu(SiO_4)(PO_4)_5F_2$. At this level we can wonder what could be the crystallographic characteristics of a continuous solution of Pu^{3+}, similar to that of Nd^{3+}, for $1 \le y \le 6$. Hence, the lattice parameters and volumes for $Ca_{10-y}Pu_y(SiO_4)_y(PO_4)_{6-y}F_2$ have been calculated, within the approximation of the established force field, and presented in Table 8. For the Pu-britholites, the unit cell volume variation with respect to y is less significant than that of the Nd-britholites $Ca_{10-y}Nd_y(SiO_4)_y(PO_4)_{6-y}F_2$ (Table 6). This cannot be attributed only to the ionic radius difference between Pu^{3+} (1.01−1.03 Å) and that of Nd^{3+} (1.03 Å), as they are almost equal, but also to the specific difference of the $Pu^{3+}{}_{core}-F_{core}$ and $Nd^{3+}{}_{core}-F_{core}$ short-range potentials. In fact, because plutonium has the tendency to substitute for Ca(2) in the fluorine tunnel and because the $Pu^{3+}{}_{core}-F_{core}$ potential is less repulsive than the $Nd^{3+}{}_{core}-F_{core}$ one, the fluorine ions are attracted toward plutonium resulting in a shrinking of the Pu-britholites cell volumes compared to the Nd-britholites ones.

The bulk modulus of the Pu-britholites as well as the C_V, C_P, and S_{vib} are calculated at 300 K and presented in Table 9. The calculated thermodynamic properties are very close to the

TABLE 9: Calculated (rounded to the nearest integer) Properties at 300 K for Pu-Britholites and for Plutonium- and Cesium-Doped Mono-silicate Nd-Britholite

	B (GPa)	C_V (J/mol K)	C_P (J/mol K)	S_{vib} (J/mol K)
$Ca_{10-y}Pu_y(SiO_4)_y(PO_4)_{6-y}F_2$				
$Ca_9Pu(SiO_4)(PO_4)_5F_2$	99	716	729	797
$Ca_8Pu_2(SiO_4)_2(PO_4)_4F_2$	105	710	722	772
$Ca_7Pu_3(SiO_4)_3(PO_4)_3F_2$	114	702	716	764
$Ca_6Pu_4(SiO_4)_4(PO_4)_2F_2$	121	694	709	759
$Ca_5Pu_5(SiO_4)_5(PO_4)F_2$	130	690	702	751
$Ca_4Pu_6(SiO_4)_6F_2$	139	682	693	738
$Ca_9(Pu^{3+})_{0.25}Nd_{0.75}(SiO_4)(PO_4)_5F_2$	99	717	733	799
$Ca_{9.25}(Pu^{4+})_{0.25}Nd_{0.5}(SiO_4)(PO_4)_5F_2$	94	722	738	805
$Ca_{9.5}Cs_{0.5}Nd_{0.5}(SiO_4)(PO_4)_5F_2$	90	724	748	810

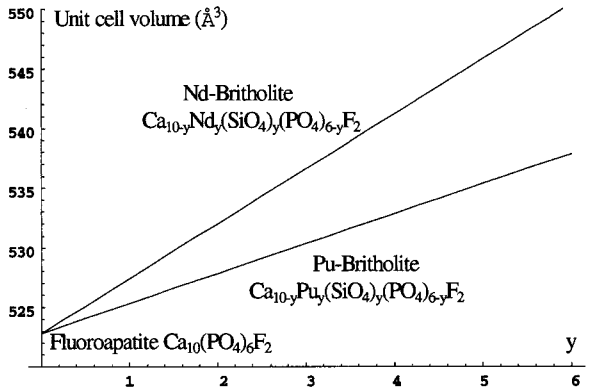

Figure 5. Unit cell volume variation of Nd-britholites and Pu-britholites with respect to the trivalent ion (Nd^{3+} or Pu^{3+}) and silicate solution, *y*.

Nd-britholites ones (Table 7). However, significant higher values for the bulk modulus are obtained for the Pu-britholites as shown in Figure 6.

Evidently, it is out of question that the Pu-britholites be used as waste forms, because of the very high plutonium concentrations which will inevitably produce high radiation damage due to α-recoil, resulting in permanent amorphization states. Conversely, the incorporation of plutonium at 6% p.w. in a mono-silicate Nd-britholite can be seriously envisioned, because the matrix will have the possibility of preserving its crystalline structure. As discussed above, depending on the synthesis conditions, plutonium could be present in that matrix in the +4 oxidation state corresponding to $Ca_{9.25}(Pu^{4+})_{0.25}Nd_{0.5}(SiO_4)(PO_4)_5F_2$. The free energy calculation, using the energy minimized unit cell $Ca_{74}(Pu^{4+})_2Nd_4(SiO_4)_8(PO_4)_{40}F_{16}$ with the Pu^{4+} ions occupying successively Ca(1) and Ca(2) demonstrates again the tendency for plutonium to substitute for Ca(2), as represented in Figure 7.

$$A_{300K}[Pu^{4+}\text{ at Ca(1)}] - A_{300K}[Pu^{4+}\text{ at Ca(2)}] = +342.8\text{ kJ/mol} \quad (10)$$

The calculated values of the bulk modulus, the vibration entropy S_{vib}, and the specific heats, C_P and C_v, for both plutonium-doped compositions, $Ca_{9.25}(Pu^{4+})_{0.25}Nd_{0.5}(SiO_4)(PO_4)_5F_2$ and $Ca_9(Pu^{3+})_{0.25}Nd_{0.75}(SiO_4)(PO_4)_5F_2$, are given in Table 9. Comparing with those of the mono-silicate Nd-britholite (Table 6), it is of great importance to notice that at up to 6% p.w. of plutonium concentration the matrix essentially preserves its mechanical and thermodynamic properties.

Similar calculations for cesium incorporation in the mono-silicate Nd-britholite using the unit cells $Ca_{76}Cs_4Nd_4(SiO_4)_8(PO_4)_{40}F_{16}$, corresponding to the composition $Ca_{9.5}Cs_{0.5}Nd_{0.5}(SiO_4)(PO_4)_5F_2$, show that Cs^+ will rather have a slight preference for Ca(1) site:

$$A_{300K}[Cs^+\text{ at Ca(1)}] - A_{300K}[Cs^+\text{ at Ca(2)}] = -44.2\text{ kJ/mol} \quad (11)$$

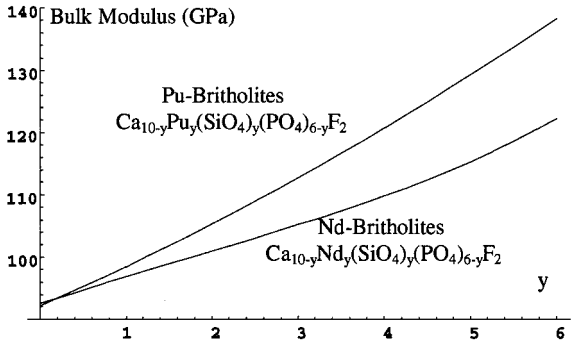

Figure 6. Bulk modulus of Nd-britholites and Pu-britholites with respect to the trivalent ion (Nd^{3+} or Pu^{3+}) and silicate solution, *y*.

The calculated properties of the cesium-doped mono-silicate Nd-britholite are also reported in Table 9. There is not a significant variation of the specific heats with respect to the matrix. However, a considerable decrease, of about 10%, of the bulk modulus should be expected.

Finally, the results of the above calculations on the preferential substitution site, Ca(1) or Ca(2), when Pu^{3+}(ionic radius 1.01−1.03 Å), Pu^{4+} (ionic radius 0.90 Å) or Cs^+ (ionic radius 1.65−1.74 Å)[29] are introduced selectively in Nd-britholites support the thesis advanced by Blasse[25] and Lin[26,27] based upon experimental observations and electrostatic considerations. According to their theory, in britholites, small and highly charged cations will preferentially substitute for Ca(2), while voluminous cations with a low charge will prefer Ca(1).

IV. Lattice Migration Energies for Plutonium and Cesium in $Ca_9Nd(SiO_4)(PO_4)_5F_2$

It is well-known that despite the fact that britholites can be synthesized under rigorous conditions, the presence of defects in the crystalline structure is inevitable. Because actinides readily substitute for calcium it is of crucial importance to examine the formation of Ca Frenkel defects as well as the Pu and Cs migration energies toward adjacent calcium vacancies. The defect formation energies can be estimated, within the Mott−Littleton approximation, by calculating the difference between the lattice energy of the perfect bulk and that containing the defect.[30] A correction for the energy of missing species at infinite distance has to be considered in the general case. However, for individual ion defects, such a correction is needless as the ion interaction potentials are defined with respect to zero energy at infinity.

For $Ca_9Nd(SiO_4)(PO_4)_5F_2$ the following defect formation energies have been calculated, corresponding to a calcium pure vacancy, with the ion at infinite distance from the crystal, and to a calcium Frenkel defect:[31]

$$E[V''_{Ca(1)}] = 24.4\text{ eV};\quad E_{\text{Frenkel}}[V''_{Ca(1)} + Ca^{2+}\text{ interstitial}] = 2.1\text{ eV} \quad (12)$$

$$E[V''_{Ca(2)}] = 25.1\text{ eV};\quad E_{\text{Frenkel}}[V''_{Ca(2)} + Ca^{2+}\text{ interstitial}] = 2.8\text{ eV} \quad (13)$$

In both cases it appears that more energy is needed to remove a Ca^{2+} from the Ca(2) site than from Ca(1). Now, the possibility

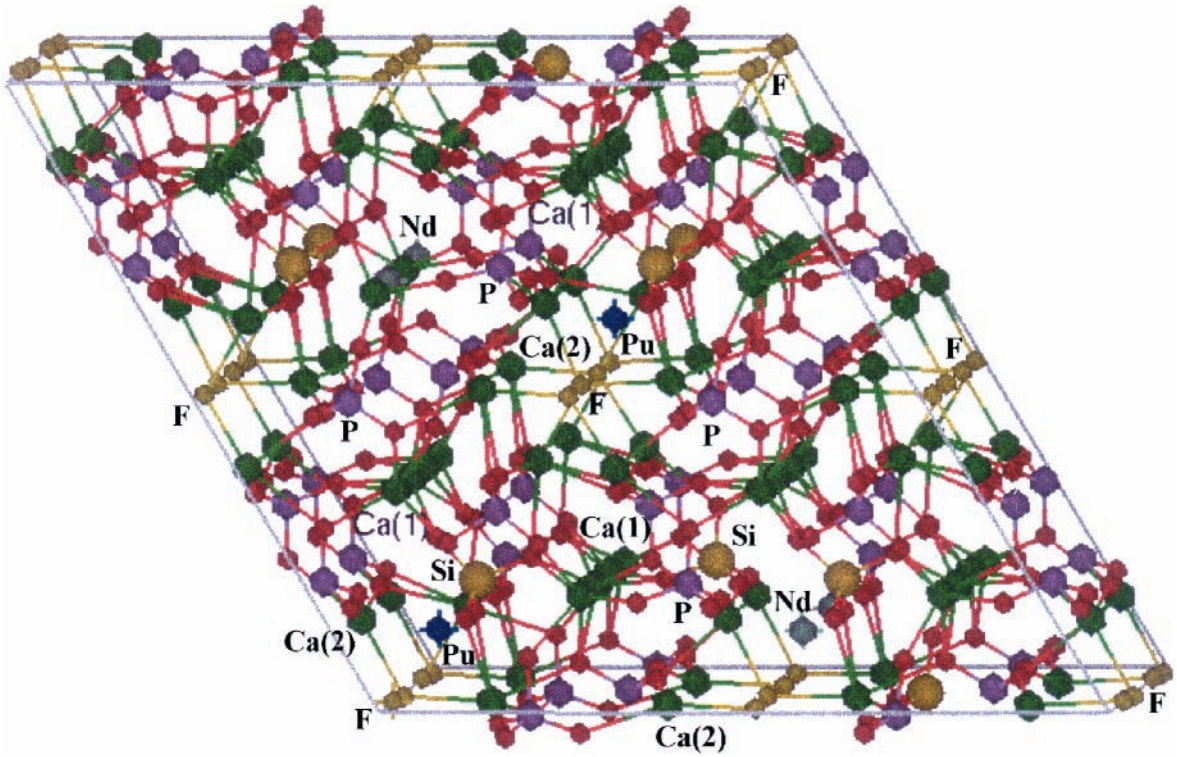

Figure 7. Plutonium-doped Nd-britholite $Ca_{9.25}Pu_{0.25}Nd_{0.5}(SiO_4)(PO_4)_5F_2$ at 6% p.w. The plutonium ions preferentially occupy calcium sites Ca(2) in the fluorine tunnel.

TABLE 10: Migration Energies for Lattice Diffusion of Pu^{4+}, Pu^{3+}, and Cs^+ in the Corresponding Mono-silicate Nd-Britholite-Doped Compositions $Ca_{9.5}Cs_{0.5}Nd_{0.5}(SiO_4)(PO_4)_5F_2$, $Ca_9(Pu^{3+})_{0.25}Nd_{0.75}(SiO_4)(PO_4)_5F_2$, and $Ca_{9.25}(Pu^{4+})_{0.25}Nd_{0.5}(SiO_4)(PO_4)_5F_2$

ion	from site Ca(2) → $V''_{Ca(2)}$	from site Ca(2) → $V''_{Ca(1)}$	from site Ca(1) → $V''_{Ca(1)}$
Pu^{4+}	2.7 eV	5.9 eV	3.1 eV
Pu^{3+}	2.1 eV	3.2 eV	2.4 eV
Cs^+	1.5 eV	1.8 eV	1.4 eV

of plutonium and cesium to move from their equilibrium positions to adjacent calcium vacancies can be analyzed by calculating the corresponding migration energies. The latter represent the potential barrier the ion has to overcome moving toward the adjacent vacancy at Ca(1) or at Ca(2) position and is obtained by the difference between the potential energy when the ion is at the stable site and that when it is on the saddle point. When analytical second derivatives of the energy are available, the saddle point research can be carried out within static lattice theory by the rational function optimization (RFO) method (eigenvector following),[32] as implemented in GULP. Application of this method for the migration of Cs^+, Pu^{3+}, and Pu^{4+}, respectively, in the compositions $Ca_{9.5}Cs_{0.5}Nd_{0.5}(SiO_4)(PO_4)_5F_2$, $Ca_9(Pu^{3+})_{0.25}Nd_{0.75}(SiO_4)(PO_4)_5F_2$ and $Ca_{9.25}(Pu^{4+})_{0.25}Nd_{0.5}(SiO_4)(PO_4)_5F_2$ gives the results presented in Table 10.

Plutonium, in a trivalent or tetravalent oxidation state will have the tendency not only to substitute for Ca(2) but also to migrate more easily from Ca(2) to Ca(2) sites around the fluorine array in the tunnel. Cesium is expected to have a considerably greater mobility as the migration energies are of about 1.5 eV, whatever the site of the adjacent calcium vacancy.

Conclusion

Based upon experimental data, fluoroapatite and neodymium britholites have been modeled using analytical potentials. Plutonium and cesium introduced selectively in a mono-silicate Nd-britholite will substitute for calcium at sites Ca(2) and Ca(1), respectively, though for cesium this tendency seems to be rather weak. Up to 6% p.w of plutonium or cesium concentration the matrix essentially preserves its mechanical and thermodynamic properties. However, a decrease of about 10% of the bulk modulus should be expected for the cesium-doped neodymium britholites. In the presence of calcium vacancies, Pu^{3+} as well as Pu^{4+} will have the tendency to migrate from Ca(2) site to Ca(2), as the corresponding lattice migration energies are much lower than those characterizing the transition from Ca(2) site to Ca(1). Consequently, significant plutonium concentrations should be expected around the fluorine arrays, in the apatite tunnels. Conversely, cesium is expected to have an important mobility in the presence of calcium vacancies, because of the lower migration energies, and should be expected to be located uniformly in the bulk. Finally, the synthesis of plutonium-doped mono-silicate neodymium britholite, at 6% p.w, with plutonium in the tetravalent oxidation state $Ca_{9.25}(Pu^{4+})_{0.25}Nd_{0.5}(SiO_4)(PO_4)_5F_2$ should correspond to a quite stable phase for plutonium immobilization.

Acknowledgment. J.D.G. would like to thank the Royal Society for a University Research Fellowship and EPSRC for the provision of computer facilities.

References and Notes

(1) Bros, R.; Carpen, J.; Sere, V.; Beltritti, A. *Radiochim. Acta* **1996**, *74*, 277.

(2) Carpena, J.; Sère, V. *Proceedings of the fourth joint EC−CEA final meeting, Saclay* **1995**, 225−238.

(3) Wagner, G. A.; Reimer, G. M. *Earth Planet. Sci. Lett.* **1972**, *14*, 263.

(4) Ewing, R. C.; Weber, W. J.; Wang, L. M. *J. Mater. Res.* **1994**, *9*, 688.

(5) Weber, W. J.; Wang, L. M. *Nucl. Instrum. Methods Phys. Res., B* **1994**, *91*, 63.

(6) Carpena, J.; Lacout, J. L. *Licence* **1993**.

(7) Ewing, R. C.; Weber, W. J.; Lutze, W. In *Disposal of Weapons Plutonium*; Merz, E. R., Walter, C. E., Eds.; Kluwer Academic Publishers: The Netherlands, 1996; p 65.
(8) Boyer, L.; Carpena, J.; Lacout, J. L. *Licence* **1998**.
(9) Meldrum, A.; Wang, L. M.; Ewing, R. C. *Nucl. Instrum. Methods Phys. Res., B* **1996**, *116*, 220.
(10) Carpena J. In *Advances in fission track geochronology*; 1998, Van den Haute, P., de Corte, Eds.; Kluwer Academic Publishers: New York, pp 91−92.
(11) Carpena, J.; Kienast, J. R.; Ouzegane, K.; Jehanno, C. *Geol. Soc. Am. Bull.* **1988**, *100*, 1237.
(12) Boyer, L.; Piriou, M.; Carpena, J.; Lacout, J. L. *Luminescence J.* Submitted.
(13) Sudarsanan, K.; Mackie, P. E.; Young, R. A. *Mater. Res. Bull.* **1972**, *7*, 1331−1338.
(14) Boyer, L. Thesis, July 7, 1998. Institut National Polytechnique de Toulouse, France.
(15) Boyer, L.; Carpena, J.; Lacout, J. L. *Solid State Ionics* **1996**, *95*, 121.
(16) Dick, B. G.; Overhauser, A. W. *Phys. Rev.* **1958**, *112*, 90.
(17) Hearnon, R. F. S. *Adv. Phys.* **1956**, *5*, 323.
(18) Gale, J. D. *Philos. Mag*. **1996**, *B73*, 3.
(19) Catlow, C. R. A. *Proc. R. Soc. Lond*. **1997**, *A353*, 533.
(20) Catlow, C. R. A.; Diller, K. M.; Norgett, M. J. *J. Phys. C: Solid State Physics* **1979**, *10*, 1395.
(21) D'Arco, S.; Islam, M. S. *Phys. Rev. B* **1997**, *B55*, 3141.
(22) Gale, J. D. *J. Chem. Soc., Faraday Trans*. **1997**, *93*, 629.
(23) Meis, C.; Gale, J. D. *Mater. Sci. Eng. B* **1998**, *57*, 52−61.
(24) Lewis, G. V.; Catlow, C. R. A. *J. Phys.* **1985**, *C18*, 1149−1161.
(25) Blasse, G. J. *Solid State Chem.* **1975**, *14*, 181.
(26) Lin J.; Su, Q. *J. Alloys Compd.* **1994**, *210*, 159.
(27) Lin, J.; Su, Q. *Mater. Chem. Phys.* **1994**, *38*, 98.
(28) Boyer, L.; Savariault, J. M.; Carpena, J.; Lacout, J. L. *Acta Crystallogr. C* **1998**, *C54*, 1057.
(29) Handbook of the physicochemical properties of the elements; Samsonov, G. V., Ed.; IFI/Plenum: New York-Washington, 1968.
(30) Mott N. F.; Littleton M. J. *Trans. Faraday Soc.* **1938**, *34*, 485.
(31) Jost W. *Diffusion*; Academic Press: New York, 1960.
(32) Banarjee A.; Adams N.; Simons J.; Shepard R. *J. Phys. Chem*. **1985**, *89*, 52.